

UTIL: An Ultra-wideband Time-difference-of-arrival Indoor Localization Dataset

The International Journal of Robotics Research
XX(X):1–7
©The Author(s) 2022
Reprints and permission:
sagepub.co.uk/journalsPermissions.nav
DOI: 10.1177/ToBeAssigned
www.sagepub.com/



Wenda Zhao¹, Abhishek Goudar¹, Xinyuan Qiao¹, and Angela P. Schoellig¹

Abstract

This paper presents an ultra-wideband (UWB) time-difference-of-arrival (TDOA) dataset collected from a quadrotor for research purposes. The dataset consists of low-level signal information from static experiments and UWB TDOA measurements and additional onboard sensor data from flight experiments on a quadrotor. The data collection process is discussed in detail, including the equipment used, measurement collection procedure, and the calibration of the quadrotor platform. All the data is made available as plain text files and we provide both Matlab and Python scripts to parse and analyze the data. We provide a thorough description of the data format and some pointers on the potential usage of each sub-dataset. The dataset is available for download at <https://utiasdsl.github.io/util-uwbdataset/>. We hope this dataset will help researchers develop and compare reliable estimation methods for the emerging UWB TDOA-based indoor localization technology.

Keywords

Ultra-wideband, time-difference-of-arrival, indoor localization

1 Introduction

Accurate indoor localization is a crucial enabling technology for many robotics applications, from warehouse management to monitoring tasks. Ultra-wideband (UWB) time-difference-of-arrival (TDOA)-based localization is a promising lightweight and low-cost solution that can scale to a large number of devices [Hamer and D’Andrea \(2018\)](#); [Zhao et al. \(2021\)](#). However, in indoor scenarios, UWB measurements are affected by non-line-of-sight (NLOS) and multipath radio propagation. Even line-of-sight (LOS) measurements exhibit error patterns, which are typically caused by the UWB antenna’s radiation characteristic [Tiemann et al. \(2017\)](#). Therefore, new algorithms are required to cope with the UWB TDOA measurement errors and noises so as to achieve accurate positioning in cluttered and harsh environments. For this purpose, we present a comprehensive UWB TDOA dataset produced in the *University of Toronto Institute for Aerospace Studies (UTIAS)*. The dataset consists of low-level signal information from static experiments (*static dataset*) and UWB TDOA measurements and additional sensor data from flight experiments on a quadrotor platform (*flight dataset*). We collected the flight dataset using four different UWB setups, also called constellations, in a variety of LOS and NLOS conditions. The sensor data were logged on-board the quadrotor with accurate timestamps during flights. By using a 10-camera Vicon motion capture system, we obtained a millimeter-level accurate ground truth data.

The intended users of this dataset are researchers who are interested in UWB TDOA-based localization. More specifically, the dataset can be used to model the UWB TDOA measurement errors under various LOS and NLOS conditions, assess the performance of UWB TDOA-based indoor localization, and design estimation algorithms to cope with the measurement errors for accurate indoor positioning.

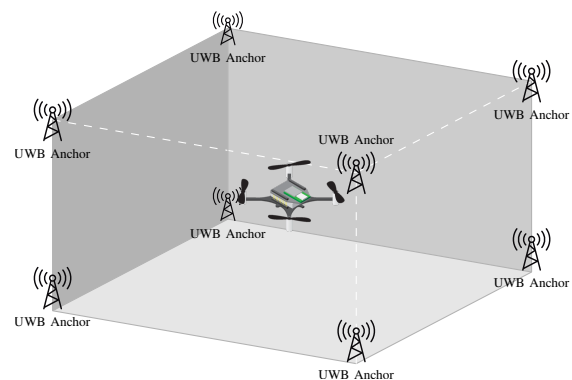


Figure 1. Sketch of an UWB TDOA localization system. UWB anchors are pre-installed with known positions in the space. The robot equipped with an UWB tag receives TDOA measurements from the anchors for localization.

Users can access the dataset via the website: <https://utiasdsl.github.io/util-uwbdataset/>.

2 UWB TDOA-based localization system

Our UWB TDOA-based localization system is sketched in Figure 1. UWB radios, called anchors, are pre-installed in the space and their positions surveyed using a total station [Leica \(2021\)](#). The robot equipped with an UWB radio, also called

¹Institute for Aerospace Studies, University of Toronto, Canada

Corresponding author:

Wenda Zhao, University of Toronto Institute for Aerospace Studies, Toronto, Ontario, M3H 5T6, Canada.

Email: wenda.zhao@robotics.utias.utoronto.ca

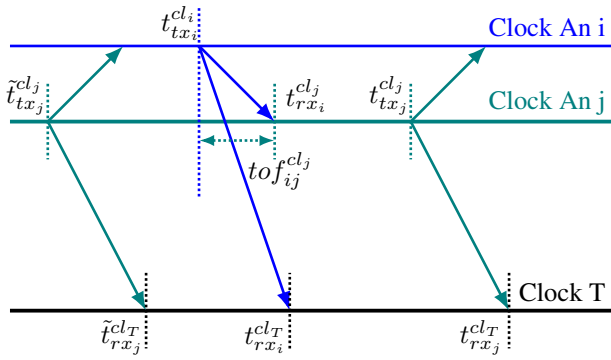


Figure 2. The sequence of UWB radio packets between the tag and anchor i and anchor j . The clocks of anchor i , anchor j , and the tag are indicated as solid lines with different colors. The radio packets between the tag and anchors are denoted as solid arrow lines.

tag, computes the difference of the UWB signal arrival times from two anchors: a TDOA measurement is the difference of the distances between the robot and the two transmitting anchors, which is proportional to the difference in signal arrival times. To better explain the content and usage of the static dataset, we introduce the UWB radio hardware used for data collection and provide a brief explanation of the TDOA principles.

2.1 UWB sensor

We use the Decawave DWM1000 [Decaware \(2016\)](#) UWB radio sensors in this dataset. The Decawave DWM1000 module is a low-cost UWB radio often used to develop cost-effective localization solutions. The Loco Positioning System (LPS) from [Bitcraze \(2021\)](#) based on DWM1000 UWB modules is used to collect UWB TDOA measurements.

Both centralized TDOA (TDOA 2) and decentralized TDOA (TDOA 3) [Meng et al. \(2016\)](#) are implemented in LPS. In centralized TDOA systems, all the anchors are synchronized w.r.t. one master anchor and the TDOA measurements are expressed in the same clock. However, centralized TDOA systems are limited by the communication constraints and suffer from single point failure [Ennasr et al. \(2016\)](#). In decentralized TDOA systems, anchors synchronize the timescales between anchor pairs, leading to less accurate TDOA measurements. Therefore, decentralized TDOA systems achieve scalability at the cost of measurement accuracy.

In the static dataset, since only two anchors are used for data collection, we ignore the difference between the centralized and decentralized TDOA modes and set the anchors into decentralized mode (TDOA 3) for testing. For the flight experiments, we commanded the quadrotor to fly the same trajectories with both centralized and decentralized TDOA modes for comparison.

2.2 Time-difference-of-arrival principles

In this subsection, we briefly explain the TDOA principles implemented in LPS. The sequence of the UWB radio packets among two anchors, anchor i and anchor j , and one tag are visualized in Figure 2. UWB radios, both anchors and



Figure 3. UWB anchors and tag for static dataset collection.

the tag, operate with their own clock, which are indicated as solid lines with different colors. A clock synchronization process is essential for an accurate computation of TDOA measurements.

We denote the clock of anchor i , anchor j , and the tag as cl_i , cl_j , and cl_T in the superscripts and the transmitting and the receiving of a radio signal from anchor i as tx_i and rx_i in the subscripts. As an example, $t_{rx_j}^{cl_T}$ indicates the receiving timestamp of radio packet from anchor j expressed in the tag's clock. We use \tilde{t} to indicate the timestamp from the previous sequence. With anchor i and anchor j at positions $\mathbf{a}_i, \mathbf{a}_j \in \mathbb{R}^3$ and one tag at position $\mathbf{p} \in \mathbb{R}^3$, the TDOA measurements from anchor i and j are computed as

$$d_{ij} = c \left[(t_{rx_j}^{cl_T} - \tilde{t}_{rx_j}^{cl_T}) - \alpha (t_{tx_j}^{cl_j} - t_{rx_i}^{cl_j} + tof_{ij}^{cl_j}) \right], \quad (1)$$

$$= \|\mathbf{p} - \mathbf{a}_j\| - \|\mathbf{p} - \mathbf{a}_i\|$$

where c indicates the speed of light, α is the clock correction parameter converting from anchor j 's clock to the tag's clock, $tof_{ij}^{cl_j}$ is the time-of-flight measurements between anchor i and anchor j expressed in anchor j 's clock, and $\|\cdot\|$ indicates the ℓ_2 norm. The clock correction parameter α is computed with the timestamps from the previous sequence

$$\alpha = \frac{t_{rx_j}^{cl_T} - \tilde{t}_{rx_j}^{cl_T}}{t_{tx_j}^{cl_j} - \tilde{t}_{tx_j}^{cl_j}}. \quad (2)$$

3 Static dataset

For the static experiments, we collected UWB TDOA measurements under various LOS and NLOS conditions. Two UWB anchors and one Crazyflie nano-quadrotor equipped with an UWB tag were placed on wooden structures, as shown in Figure 3. For clarity, the two UWB anchors are referred to as anchor 1 and anchor 2, respectively. A millimeter-level accurate Vicron motion capture system measures the poses of the tag and the anchors for ground truth data. Since timestamps are not critical for static signal testing, we logged the static TDOA measurement data through Robot Operating System (ROS). In this section, we provide the information of the LOS and NLOS static tests. The format and descriptions of each sub-dataset are provided in Section 3.3.

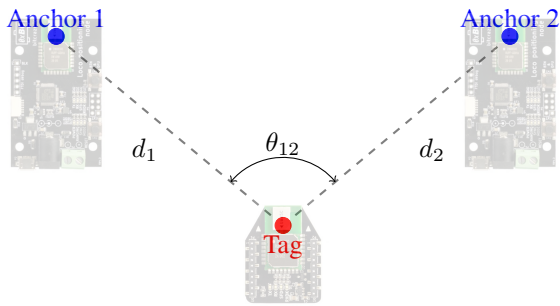


Figure 4. A diagram of the setup of UWB LOS experiments.

3.1 Line-of-sight tests

In LOS conditions, we collected data from two tests: (i) the LOS distance test and (ii) the LOS angle test. As sketched in Figure 4, the angle between two anchors is denoted as θ_{12} and the distance between the tag and anchor 1 and 2 are indicated as d_1 and d_2 , respectively. The positions of the tag and anchor 2 are fixed throughout the LOS data collection process. In LOS distance test, we change the distance d_1 from 0.5 meter to 6.5 meters with an interval of 0.5 meter. In LOS angle test, we change the angle θ_{12} from 180° to 15° with an interval of 15° .

3.2 None-line-of-sight tests

During the NLOS tests, we fixed the positions of the tag and two anchors and placed different obstacles to block the line-of-sight of TDOA measurements. Four reflective markers were placed on the top surface of the obstacle to indicate its position during the experiments. To reflect the comprehensive performance of UWB NLOS measurements, we selected six obstacles of different type of materials commonly used in indoor settings (see Figure 5), including cardboard, metal, wood, plastic, and foam.

As explained in Section 2.2, the UWB tag listens to the radio packets transmitting between anchors to compute TDOA measurements. Both NLOS conditions between one anchor and the tag and between two anchors will affect TDOA measurements. Therefore, we conducted NLOS experiments under (i) NLOS conditions between anchor 1 and the tag and (ii) NLOS conditions between anchor 1 and anchor 2. Considering the different radio reflection and diffraction effects with one obstacle under different orientations, we collect six sub-datasets for each NLOS condition with different orientations of the obstacle. One LOS data is collected for comparison.

3.3 Static dataset format

During each static experiment, we collected the signal-to-noise ratio (SNR) and power difference (P_d) values provided in the user manual Decawave (2017) as the metrics to assess the quality of received UWB signals. The computation of SNR and power difference P_d are as follows

$$\text{SNR} = \frac{Am_f}{\sigma_n}, \quad P_d = P_r - P_f, \quad (3)$$

where Am_f indicates the *First Path Amplitude value*, σ_n indicates the *Standard Deviation of Channel Impulse*

Table 1. Format of the .csv file in each static sub-dataset.

CSV Column	Value	Description
1	d_{12} [m]	TDOA measurements $d_{12} = d_2 - d_1$
2	d_{21} [m]	TDOA measurements $d_{21} = d_1 - d_2$
3	SNR_1	SNR value of the UWB radio packet sent from An 1 received by the tag
4	P_{d1} [dB]	power difference value of the UWB radio packet sent from An 1 received by the tag
5	SNR_2	SNR value of the UWB radio packet sent from An 2 received by the tag
6	P_{d2} [dB]	power difference value of the UWB radio packet sent from An 2 received by the tag
7	SNR^{an1}	SNR value of the UWB radio packet sent from An 2 received by An 1
8	P_d^{an1} [dB]	power difference value of the UWB radio packet sent from An 2 received by An 1
9	r_{12}^{cl1} [m]	distance between An 1 and An 2 computed by tof_{12}^{cl1}
10	SNR^{an2}	SNR value of the UWB radio packet sent from An 1 received by An 2
11	P_d^{an2} [dB]	power difference value of the UWB radio packet sent from An 1 received by An 2
12	r_{12}^{cl2} [m]	distance between An 1 and An 2 computed by tof_{12}^{cl2}

Response Estimate Noise value, and P_r and P_f are the total received power and the first path power, respectively. In general, a higher SNR value or a lower P_d indicates the received radio signal is of good quality Decawave (2017). The four raw measurements $\{Am_f, \sigma_n, P_r, P_f\}$ can be accessed from the DW1000 chip when receiving an UWB signal. We refer to Section 4.7 of the user manual Decawave (2017) for detailed information.

In each sub-dataset, we provide a .csv file containing the collected data and a .txt file containing the poses of the tag and two anchors in one folder. For NLOS tests, the positions of the four markers on the obstacles are also included in the .txt file. The format of the .csv file and brief descriptions of each value are summarized in Table 1. The format of the position data provided in the .txt file is (x, y, z) in meters. The orientation is provided as a unit quaternion (q_x, q_y, q_z, q_w) , where q_w and (q_x, q_y, q_z) are the scalar and the vector components, respectively. We provide both Matlab and Python scripts (see Table 4) to parse the data.

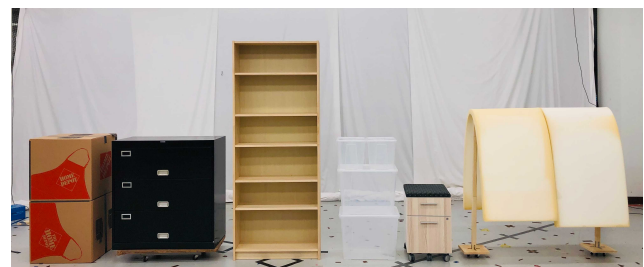


Figure 5. Obstacles used in the NLOS tests. The material of the obstacle from left to right are cardboard, metal, wood, plastic, wood, and foam.

Table 2. Summary of the static dataset. Each folder consists of a `.csv` file containing the signal testing data and a `.txt` file containing the ground truth poses of the tag and two anchors. For NLOS tests, the positions of the four markers on the obstacle are also provided in the `.txt` file.

Folder name (base folder: <code>./dataset/static-dataset/</code>)	Description
<code>los/angleTest/angleT_{1~12}/</code>	Folders containing the data of the 12 LOS angle tests.
<code>los/distTest/distT_{1~12}/</code>	Folders containing the data of the 12 LOS distance tests.
<code>nlos/anAn/cardboard/data_{1~6}/</code>	Folders containing the data of the 6 NLOS tests between anchor 1 and anchor 2 with cardboard boxes.
<code>nlos/anAn/foam/data_{1~6}/</code>	Folders containing the data of the 6 NLOS tests between anchor 1 and anchor 2 with foam mattresses.
<code>nlos/anAn/metal/data_{1~6}/</code>	Folders containing the data of the 6 NLOS tests between anchor 1 and anchor 2 with a metal cabinet.
<code>nlos/anAn/plastic/data_{1~6}/</code>	Folders containing the data of the 6 NLOS tests between anchor 1 and anchor 2 with plastic boxes.
<code>nlos/anAn/wooden-cabinet/data_{1~6}/</code>	Folders containing the data of the 6 NLOS tests between anchor 1 and anchor 2 with a wooden cabinet.
<code>nlos/anAn/wooden-shelf/data_{1~6}/</code>	Folders containing the data of the 6 NLOS tests between anchor 1 and anchor 2 with a wooden shelf.
<code>nlos/anTag/cardboard/data_{1~6}/</code>	Folders containing the data of the 6 NLOS tests between anchor 1 and the tag with cardboard boxes.
<code>nlos/anTag/foam/data_{1~6}/</code>	Folders containing the data of the 6 NLOS tests between anchor 1 and the tag with foam mattresses.
<code>nlos/anTag/metal/data_{1~6}/</code>	Folders containing the data of the 6 NLOS tests between anchor 1 and the tag with a metal cabinet.
<code>nlos/anTag/metal/data-mp/</code>	Folders containing the data of the 6 NLOS tests between anchor 1 and the tag with a metal cabinet. In this test, the tag received a multi-path signal due to the severe NLOS condition.
<code>nlos/anTag/plastic/data_{1~6}/</code>	Folders containing the data of the 6 NLOS tests between anchor 1 and the tag with plastic boxes.
<code>nlos/anTag/wooden-cabinet/data_{1~6}/</code>	Folders containing the data of the 6 NLOS tests between anchor 1 and the tag with a wooden cabinet.
<code>nlos/anTag/wooden-shelf/data_{1~6}/</code>	Folders containing the data of the 6 NLOS tests between anchor 1 and the tag with a wooden shelf.
<code>nlos/anTag/los-data/</code>	Folder containing the LOS data to compare against NLOS testing results.

The descriptions of each static sub-dataset is summarized in Table 2.

measurement biases [Zhao et al. \(2021\)](#); [Ledergerber and](#)

4 Flight dataset

In this section, we provide a detailed description about the data collected during the flight experiments.

4.1 Flight arena and experimental setup

The UWB TDOA flight dataset is produced in an indoor flight arena measuring approximately $7.0\text{ m} \times 8.0\text{ m} \times 3.5\text{ m}$ and is equipped with a motion capture system of 10 Vicon Vantage+ cameras. Printed Apriltags are attached to the soft mattresses to provide visual features for optical flow. Figure 6 is a photograph of our flight arena during data collection.

For each sub-dataset, eight UWB anchors were pre-installed in the flight arena referred to as a constellation. Three different UWB constellations are used for data collection. Each UWB anchor is mounted to a 3D printed stand with three extended arms (see Figure 6). Since the low-cost DW1000 UWB chip is reported to have pose-related

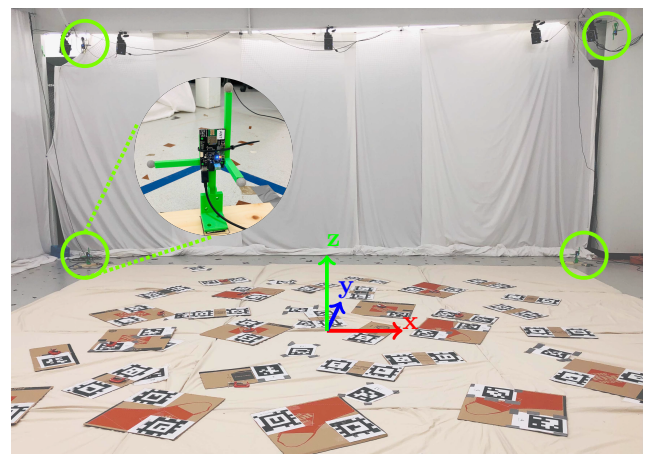


Figure 6. A photo of the flight arena. The UWB anchors are enclosed with green circles. The ground is covered with soft mattresses with a thickness of two inches (5.08 cm). Printed Apriltags are attached to the mattresses to provide visual features for the optical flow.

D’Andrea (2017), we use a mm-level accurate Leica total station to survey the position and the orientation of each anchor for reproducibility.

We refer to the Vicon frame (see Figure 6) as the inertial frame. To align the Leica total station frame and the inertial frame, we use the total station to survey six Vicon reflective markers with known positions in inertial frame and compute the transformation matrix through point cloud alignment. To assess the quality of the frame alignment between the total station and the vicon, we compute the reprojection error of the six reflective markers. All the survey points in the total station frame are converted into the inertial frame with a root-mean-squared error (RMSE) of around 1.12 mm.

We use the total station to survey the center of the UWB antenna as anchor position and the three markers on the extended arms in the total station frame. Then, we convert the survey results into the inertial frame to compute the anchor pose expressed in the inertial frame. We measure the positions of the three markers in the anchor body frame manually with a ruler and compute the transformation matrix from the anchor body frame to the inertial frame through point cloud alignment. The position (x, y, z) in meters and orientation expressed in unit quaternion (q_x, q_y, q_z, q_w) for each anchor in the inertial frame are computed through the `anchor_survey.m(py)` scripts.

4.2 Quadrotor platform

We built a customized quadrotor based on the Crazyflie Bolt flight controller with an inertial measurement unit (IMU) and attached commercially available extension boards (so-called decks) from Bitcraze for data collection (see Figure 8). The LPS UWB tag is mounted vertically on the top since the DW1000 antenna radiation pattern is uniform in its azimuth plane Decaware (2016). The STL files for the quadrotor frame and the UWB tag support are provided in the `setup_files/stl-files` folder (see Table 4). A flow deck attached at the bottom provides optical flow measurements and a laser-based time-of-flight (ToF) sensor provides the local altitude information. The accelerometer and gyroscope data is obtained from the onboard IMU. A micro SD card deck logs the raw sensor data received by the flight control board with high-precision microsecond timestamps. The customized quadrotor communicates with a ground station computer over a 2.4 GHz USB radio

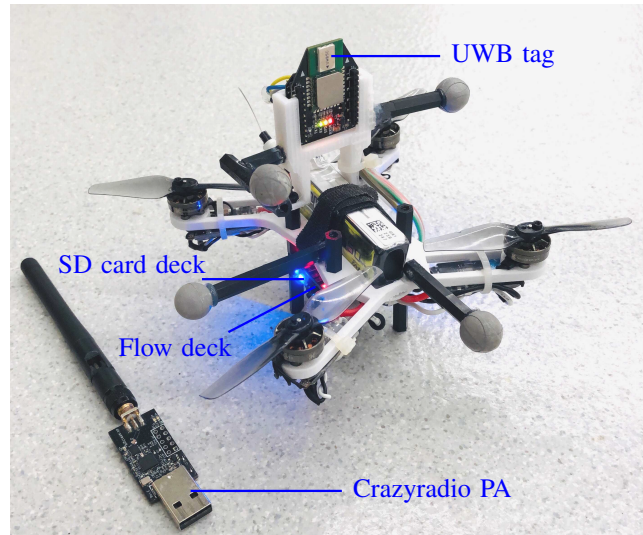


Figure 8. The customized quadrotor platform based on the Crazyflie Bolt flight controller.

dongle (Crazyradio PA) for high-level interaction. In terms of software, we use the Crazyswarm package Preiss et al. (2017) to send high-level commands, such as takeoff/landing and start/stop of data logging, pre-defined waypoints, and the pose of the quadrotor measured by the motion capture system to the quadrotor.

We operate the motion capture system at a fixed sample frequency of 200 Hz and send the measured quadrotor pose to the onboard extended Kalman filter (EKF) with a small variance, 0.001 m for position and 0.0005 for quaternion, for state estimation. Onboard the quadrotor, the raw UWB measurements, gyroscope, accelerometer, optical flow, ToF laser-ranging, barometer, and the Vicon pose measurements (sent from the ground station) are recorded as event streams. The Vicon pose measurements logged onboard are treated as the ground truth data. Each datapoint is timestamped with the onboard microsecond timer and the resulting time series are written to the micro SD card as a binary file. Python scripts are provided to parse and analyze the binary data.

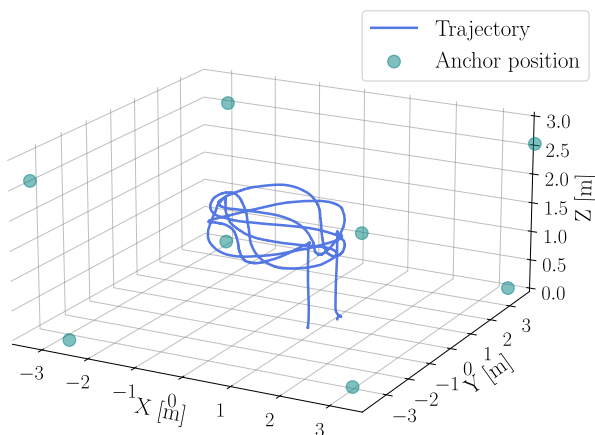


Figure 7. Trajectory of sub-dataset 3, constellation 1.

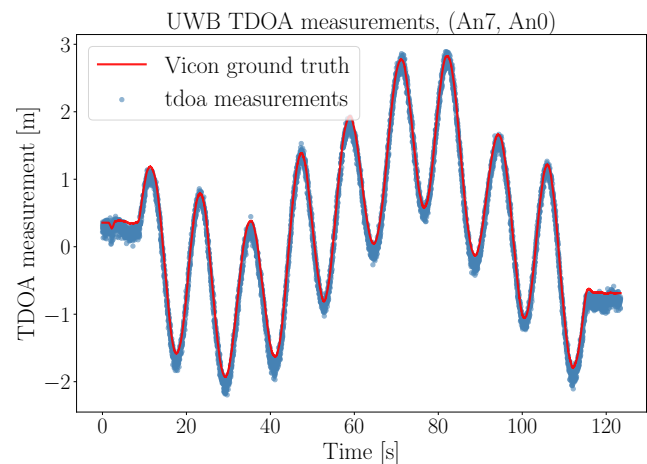


Figure 9. UWB TDOA measurements d_{07} in sub-dataset 3, constellation 1.

Table 3. Summary of the flight dataset format

CSV column	Name	Format
1 ~ 4	TDOA	(timestamp [ms], An-ID i , An-ID j , d_{ij} [m])
5 ~ 8	Acceleration	(timestamp [ms], acc x [G], acc y [G], acc z [G])
9 ~ 12	Gyroscope	(timestamp [ms], gyo x [deg/s], gyo y [deg/s], gyo z [deg/s])
13 ~ 14	Tof laser-ranging	(timestamp [ms], Tof [m])
15 ~ 17	Optical flow	(timestamp [ms], dpixel x , dpixel y)
18 ~ 19	Barometer	(timestamp [ms], barometer [asl])
20 ~ 27	Ground truth pose	(timestamp [ms], x [m], y [m], z [m], q_x, q_y, q_z, q_w)

4.3 Latency

We use the method provided in [Preiss et al. \(2017\)](#) to measure the latency from the ground station software to the onboard firmware. We manually flicked the quadrotor and recorded the onboard microsecond timestamps where the acceleration and Vicon measurements show a corresponding spike. The offset between the two timestamps is the time delay of the radio communication between the ground station and the quadrotor. The system latency is tested to be around 10 ms.

4.4 Calibration

We refer to the offset between the center of a sensor and the vehicle center as sensor extrinsic parameters. We calibrated the sensor extrinsic parameters by manually measuring the translation vectors from the center of the vehicle to onboard sensors (UWB tag and flow deck). The IMU is assumed to be aligned with the vehicle center. The translation vector from the vehicle to the UWB tag is measured as $r_{uv} = [-0.012, 0.001, 0.091]^T$ m and the measurement model is:

$$d_{ij} = \|(\mathbf{C}_{iv}r_{uv} + \mathbf{p}) - \mathbf{a}_j\| - \|(\mathbf{C}_{iv}r_{uv} + \mathbf{p}) - \mathbf{a}_i\|, \quad (4)$$

where \mathbf{C}_{iv} is the rotation matrix from the vehicle frame to the inertial frame and \mathbf{p} indicates the position of the vehicle expressed in the inertial frame.

Similarly, the translation vector from the vehicle to the flow-deck extension board is measured to be $r_{fv} = [0.000, 0.000, -0.012]^T$ m. Since we cover the ground of the flight arena with 2-inch thick (0.0508 m) mattresses for protection during data collection, the thickness of the mattress needs to be taken into account while using the ToF measurements. We refer to Section 6.5 of [Greiff \(2017\)](#) for the detailed information of the flow-deck extension board.

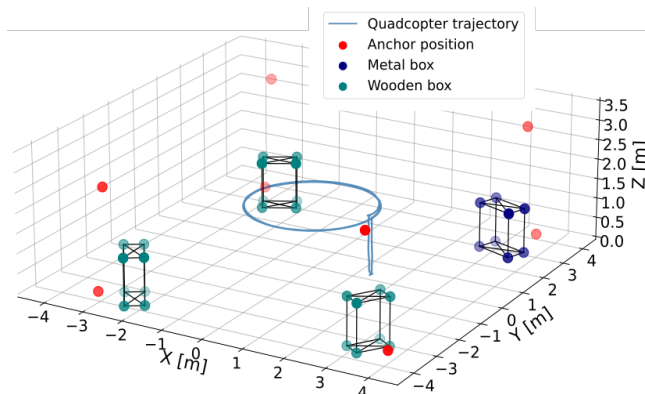


Figure 10. The experimental flight trajectory 1 in constellation 4, NLOS trial 4. A challenging NLOS condition was induced by three wooden obstacles and one metal obstacle.

Table 4. Description of the scripts provided for the dataset

File name (base folder: ./scripts/)	Description
static-dataset/ los_visual.m(py)	Scripts to visualize LOS static data.
static-dataset/ nlos_visual.m(py)	Scripts to visualize NLOS static data.
static-dataset/ los_bagTocsv.py	Script to convert LOS static data from rosbag to csv.
static-dataset/ nlos_bagTocsv.py	script to convert NLOS static data from rosbag to csv.
flight-dataset/ visual_tdoa2.m(py)	Scripts to visualize sensor data in TDOA2 mode
flight-dataset/ visual_tdoa3.m(py)	Scripts to visualize sensor data in TDOA3 mode
flight-dataset/ visual_bias.m(py)	Scripts to visualize the UWB measurement biases.
flight-dataset/ visual_obs_const3.py	Script to visualize the trajectory and positions of obstacles during manual data collections in const3.
flight-dataset/ visual_obs_const4.py	Script to visualize the trajectory and positions of the static obstacles during data collections in const4.
flight-dataset/ animations/	Animations for experiments with dynamic obstacles
flight-dataset/ sdc_card/scripts/	Folder containing Python scripts to parse the raw data (binary files).
survey/ anchor_survey.m(py)	Scripts to convert the survey results into Vicon frame.
estimation/	Folder containing an error-state Kalman filter.
../setup_files/	Folder containing SD card config file and STL files for the anchor stand, quadrotor frame, and UWB tag support.

The Crazyflie Bolt flight controller board we used does not have a high-stability crystal. As a result, the onboard clock might drift during long-term flights. However, as the length of each sub-dataset is around 120 seconds, the clock drift doesn't have a big influence for data collection.

4.5 Flight dataset format

For the flight experiments, we collected the sensor data during flights using four different UWB constellations. In constellation 1 and 2, we setup clear LOS conditions for UWB data collection. The trajectory of sub-dataset 3 with UWB constellation 1 is shown in Figure 7 and one of the TDOA measurement, d_{07} , is shown in Figure 9. In

constellation 3, the UWB measurements from anchors 3 and 6 show relatively higher noise. A potential reason is that since anchors 3 and 6 were placed close to the wall and the ceiling, the radio signals suffered from multi-path radio propagation. To simulate more realistic and challenging conditions, we collected sensor data in a variety of cluttered environments with static and dynamic obstacles in constellation 4. One challenging NLOS condition in NLOS trial 4 is demonstrated in Fig. 10 as an example. For the experiments with dynamic obstacles (trial 5 and 6), we provide corresponding animations for each experiment in the `scripts/flight-dataset/animations/` folder. A comprehensive description of each flight experiment is provided in Table 5.

For each UWB constellation, we provide the raw Leica total station survey results and computed anchor poses in `.txt` files. In each sub-dataset, we provide the timestamped accelerometer, gyroscope, UWB TDOA, optical flow, ToF laser-ranger, and the barometer measurements and the ground truth measurements of the quadrotor's pose in a `.csv` file. The data format for each sensor data is summarized in Table 3. We also provide rosbag data converted from binary files for ROS related applications. The Matlab and Python scripts provided for parsing the data are summarized in Table 4.

5 Data usage

In this section, we provide two potential usages of this dataset for users.

5.1 UWB TDOA measurement modeling

For UWB TDOA localization, modeling the measurement errors under LOS and NLOS scenarios is important for the design of localization algorithms Ruiz and Granja (2017); Prorok et al. (2012). The stationary UWB TDOA signal testing data can be used to model the distribution of the UWB TDOA measurement errors under various LOS and NLOS conditions.

5.2 Accurate UWB TDOA-based localization

The flight dataset can be used to develop UWB TDOA-based localization algorithms. We provide the UWB measurements under centralized TDOA mode (TDOA2) and decentralized TDOA mode (TDOA3). The flight dataset collected in constellation 1 and 2 can be used to compare the localization performance between different UWB modes using low-cost DWM1000 UWB modules.

It is reported in the literature that the low-cost DW1000 UWB chip suffers from systematic measurement biases Zhao et al. (2021); Ledergerber and D'Andrea (2017). Also, the UWB radio measurements are often corrupted with multi-path and NLOS signal propagation in real-world scenarios. In cluttered indoor environments, multi-path and NLOS radio propagation cannot be avoided in general. Therefore, the flight dataset collected in constellation 3 and 4 can be used to design new algorithms to cope with UWB measurement errors and noise for accurate UWB-based indoor localization.

6 Acknowledgments

We would like to thank Kristoffer Richardsson and Tobias Antonsson (Bitcraze) for their guidance on the software and hardware development of the customized quadrotor platform.

References

- Bitcraze (2021) Bitcraze Loco Positioning System. URL <https://www.bitcraze.io/documentation/system/positioning/loco-positioning-system/>.
- Decawave (2016) Decawave DW1000 datasheet. URL <https://www.decawave.com/wp-content/uploads/2020/09/DWM1000-Datasheet.pdf>.
- Decawave (2017) Decawave DW1000 user manual. URL https://www.decawave.com/sites/default/files/resources/dw1000_user_manual_2.11.pdf.
- Ennasr O, Xing G and Tan X (2016) Distributed time-difference-of-arrival (tdoa)-based localization of a moving target. In: *2016 IEEE 55th Conference on Decision and Control (CDC)*. IEEE, pp. 2652–2658.
- Greiff M (2017) *Modelling and control of the crazyflie quadrotor for aggressive and autonomous flight by optical flow driven state estimation*. Master's Thesis, Lund University.
- Hamer M and D'Andrea R (2018) Self-calibrating ultra-wideband network supporting multi-robot localization. *IEEE Access* 6: 22292–22304.
- Ledergerber A and D'Andrea R (2017) Ultra-wideband range measurement model with Gaussian processes. In: *Proc. of the IEEE Conference on Control Technology and Applications (CCTA)*. pp. 1929–1934.
- Leica G (2021) Leica Geosystems Robotic Total Station. URL <https://leica-geosystems.com/products/total-stations/robotic-total-stations>.
- Meng W, Xie L and Xiao W (2016) Optimal tdoa sensor-pair placement with uncertainty in source location. *IEEE Transactions on Vehicular Technology* 65(11): 9260–9271.
- Preiss JA, Honig W, Sukhatme GS and Ayanian N (2017) Crazyswarm: A large nano-quadcopter swarm. In: *2017 IEEE International Conference on Robotics and Automation (ICRA)*. IEEE, pp. 3299–3304.
- Prorok A, Gonon L and Martinoli A (2012) Online model estimation of ultra-wideband tdoa measurements for mobile robot localization. In: *2012 IEEE International Conference on Robotics and Automation*. Ieee, pp. 807–814.
- Ruiz ARJ and Granja FS (2017) Comparing ubisense, bespoon, and decawave uwb location systems: Indoor performance analysis. *IEEE Transactions on instrumentation and Measurement* 66(8): 2106–2117.
- Tiemann J, Pillmann J and Wietfeld C (2017) Ultra-wideband antenna-induced error prediction using deep learning on channel response data. In: *2017 IEEE 85th Vehicular Technology Conference (VTC Spring)*. IEEE, pp. 1–5.
- Zhao W, Panerati J and Schoellig AP (2021) Learning-based bias correction for time difference of arrival ultra-wideband localization of resource-constrained mobile robots. *IEEE Robotics and Automation Letters* 6(2): 3639–3646.

Table 5. Summary of the flight dataset

Folder name (base folder: ./flight-dataset/csv-data)	Description
const1/const1-trial1~6-tdoa2.csv	Log data from trajectory 1 ~ 6 in const. 1 (TDOA2 mode).
const1/const1-trial1~6-tdoa3.csv	Log data from trajectory 1 ~ 6 in const. 1 (TDOA3 mode).
const2/const2-trial1~6-tdoa2.csv	Log data from trajectory 1 ~ 6 in const. 2 (TDOA2 mode).
const2/const2-trial1~6-tdoa3.csv	Log data from trajectory 1 ~ 6 in const. 2 (TDOA3 mode).
const3/const3-trial1~7-tdoa2.csv	Log data from trajectory 1 ~ 7 in const. 3 (TDOA2 mode).
const3/const3-trial1~7-tdoa3.csv	Log data from trajectory 1 ~ 7 in const. 3 (TDOA3 mode).
const3/const3-trial8-tdoa2-manual1~2.csv	Log data through manual movements in the presence of obstacles in const. 3 (TDOA2 mode).
const3/const3-trial8-tdoa3-manual1~2.csv	Log data through manual movements in the presence of obstacles in const. 3 (TDOA3 mode).
const4/const4-trial1-tdoa2-traj1~3.csv	Log data from trajectory 1 ~ 3 in const. 4 (TDOA2 mode, LOS condition).
const4/const4-trial1-tdoa3-traj1~3.csv	Log data from trajectory 1 ~ 3 in const. 4 (TDOA3 mode, LOS condition).
const4/const4-trial2-tdoa2-traj1~3.csv	Log data from trajectory 1 ~ 3 in const. 4 (TDOA2 mode, with one wooden obstacle).
const4/const4-trial2-tdoa3-traj1~3.csv	Log data from trajectory 1 ~ 3 in const. 4 (TDOA3 mode, with one wooden obstacle).
const4/const4-trial3-tdoa2-traj1~3.csv	Log data from trajectory 1 ~ 3 in const. 4 (TDOA2 mode, with one metal obstacle).
const4/const4-trial3-tdoa3-traj1~3.csv	Log data from trajectory 1 ~ 3 in const. 4 (TDOA3 mode, with one metal obstacle).
const4/const4-trial4-tdoa2-traj1~3.csv	Log data from trajectory 1 ~ 3 in const. 4 (TDOA2 mode, with one metal and three wooden obstacles).
const4/const4-trial4-tdoa3-traj1~3.csv	Log data from trajectory 1 ~ 3 in const. 4 (TDOA3 mode, with one metal and three wooden obstacles).
const4/const4-trial5-tdoa2-traj1~3.csv	Log data from trajectory 1 ~ 3 in const. 4 (TDOA2 mode, with one dynamic metal obstacle).
const4/const4-trial5-tdoa3-traj1~3.csv	Log data from trajectory 1 ~ 3 in const. 4 (TDOA3 mode, with one dynamic metal obstacle).
const4/const4-trial6-tdoa2-traj1~3.csv	Log data from trajectory 1 ~ 3 in const. 4 (TDOA2 mode, with one dynamic metal obstacle, two static wooden obstacles).
const4/const4-trial6-tdoa3-traj1~3.csv	Log data from trajectory 1 ~ 3 in const. 4 (TDOA3 mode, with one dynamic metal obstacle, two static wooden obstacles).
const4/const4-trial7-tdoa2-manual1~3.csv	Log data through manual movements in const. 4 (TDOA2 mode, with one metal obstacle, three wooden obstacles).
../survey-results/raw-data/anchor_const1~4.txt	Raw data of the total station surveying for UWB const. 1 ~ 4
../survey-results/anchor_const1~4_survey.txt	Survey results for UWB const. 1 ~ 4
../binary-data/	Folder containing raw binary data files logged into the micro SD-card during flights.
../rosvbag-data/	Folder containing converted rosvbag data for flight dataset.